UDK 669.058.4: 629.7.036.72
Original scientific article/Izvirni znanstveni članek

ISSN 1580-2949
Mater. Tehnol.

LOAD INFLUENCE ON THE FRICTION AND WEAR BEHAVIOR OF ARC ION PLATED CR COATINGS

VPLIV OBREMENITVE NA TRENJE IN OBRABO KROMOVIH PREVLEK IZDELANIH S POSTOPKOM IONSKEGA OBLOČNEGA PLATIRANJA

Jinpeng Yang[1], Guanghui Wang[1], Haimin Yan[2], Zijun Wang[1], Cean Guo[1*], Jian Zhang[1]

[1]School of Equipment Engineering, Shenyang Ligong University, Shenyang 110159, China
[2]Ha Room 1, No.81-2 Wencui Road, Shenhe District, Shenyang 110000, China

Prejem rokopisa – received: 2024-09-21; sprejem za objavo – accepted for publication: 2025-03-26

doi:10.17222/mit.2024.1282

A Cr coating was fabricated on a CrNi3MoVA steel substrate using arc ion plating, and its friction and wear behavior was systematically investigated under loads of 3, 6 and 9 N. The results show that the load has a significant influence on the tribological properties of the Cr coating. With the increase in the load, both the friction coefficient and the wear rate of the Cr coating decrease, and the maximum equivalent stress of the rubbing zone firstly increases sharply and then decreases. A severe-to-mild adhesive wear transition takes place in the tribofilm area at the contact interface when a critical value is reached under the load of 9 N, accompanied by oxidation and hardening of the surface material of the Cr coating.

Keywords: friction and wear, Cr coating, arc ion plating, tribofilm

Avtorji opisujejo izdelavo kromovih (Cr) prevlek s tehniko ionskega obločnega platiranja na jekleno podlago vrste CrNi3MoVA. V članku nato opisujejo še sistematično raziskavo tribološkega obnašanja izdelanih prevlek pri obremenitvah (3, 6 in 9) N. Rezultati eksperimentalnih raziskav so pokazali, da obremenitev pomembno vpliva na tribološke lastnosti Cr prevleke. Z naraščajočo obremenitvijo se tako koeficient trenja kot tudi hitrost obrabe zmanjšujeta in maksimalna ekvivalentna napetost v območju drgnjenja najprej močno narašča in se nato zmanjšuje. Do prehoda med dvema mehanizmoma obrabe; močnim in blagim lepljenjem pride po nastanku območja s tribološkim filmom na vmesni ploskvi, ko je dosežena kritična vrednost obremenitve 9 N. Na tribološko obnašanje Cr prevleke vplivata istočasno tudi oksidacija in mehansko utrjevanje površine prevleke.

Ključne besede: trenje in obraba, Cr prevleka, ionsko obločno platiranje, tribološki film

1 INTRODUCTION

Chromium (Cr), usually used as a coating on a metal substrate, exhibits high hardness, as well as excellent heat, wear and corrosion resistance, meeting the engineering requirement of harsh work environments.[1–4] The usual fabrication technique for a Cr coating is electroplating, which dates back to the early 19th century.[5,6] Electroplated Cr coatings have been used in many industrial fields, such as aerospace, aviation, military, machinery, etc.[7] However, this technique also has some shortcomings, including cracks within the coating, and weak bonding strength under aggressive working conditions.[8] Especially the electroplating bath often consists of hexavalent chromium ions, which are toxic and thus prohibited in most countries; therefore, it is urgent to find a new environment-friendly alternative.[9,10]

Arc ion plating (AIP), one of the physical vapor deposition techniques, offers many advantages over electroplating for fabricating Cr coatings. Firstly, an AIP Cr coating has stronger bonding strength due to the ion bombardment effect, forming a thin metallurgical bonding interface. Secondly, the AIP Cr coating exhibits no cracks, thereby preventing corrosive media from damaging the coating-substrate system through cracks. Thirdly, the AIP technique allows better uniformity compared to the corner effect of elctroplating. Fourthly, the AIP technique allows the fabrication of a Cr-N-O or Cr alloy coating by introducing reactive gas or using a Cr alloy target. Finally, the AIP technique is environmentally friendly for fabricating Cr coatings.[11]

Recent studies found that Cr coatings fabricated with AIP exhibit excellent overall performance and show promising application potential. M. L. Shen et al. prepared a Cr coating using the AIP technique to investigate its oxidation behavior at 900 °C. The results showed that the self-ion bombardment can effectively enhance the oxidation resistance of Cr coatings, while high vacuum has a more remarkable influence on oxidation resistance than ion bombardment energy.[12] M. Hu investigated the thermal shock behavior and failure mechanisms of two types of Cr coatings prepared with electroplating and

*Corresponding author's e-mail:
bigocean1979@aliyun.com (Cean Guo)

AIP on a non-planar structure at 900 °C. The results showed that the AIP Cr coating has better uniformity and thermal shock resistance than the electroplated Cr coating.[13,14]

Wear always takes place on the surface of a component of equipment, and modern surface technologies are effective at solving wear problem.s[15–17] However, although electroplated Cr coatings have been widely applied in the field of friction and wear, and their friction and wear performance has been systematically investigated,[18—20] there are few researches on the tribological properties of AIP Cr coatings. It is well known that load has a significant influence on the tribological properties of the friction pair. This work aims to investigate the load influence on the friction and wear behavior of AIP Cr coatings, rubbing against a relatively soft material, in order to replace electroplated Cr coatings currently used in gun bores.

2 MATERIALS AND METHODS

The CrNi3MoVA steel was used for a gun barrel as the substrate material, and its chemical composition is shown in **Table 1**. The CrNi3MoVA steel was obtained for electroslag remelting and its heat treatment included normalizing at 880 °C for 60 min, quenching at 870 °C for 60 min, first tempering at 580 °C for 120 min, and second tempering at 600 °C for 120 min. The hardness of the CrNi3MoVA steel after the heat treatment was 429 HV. The surface of the CrNi3MoVA steel samples was ground step by step up to 1500 grit using SiC sandpaper and polished to a mirror finish using 2.5 μm diamond paste. The Cr coating was fabricated using the AIP technique with high-purity Cr targets (99.999 %), and its process parameters are shown in **Table 2**. For convenience in the discussion, the Cr-coated CrNi3MoVA steel is hereafter referred to as the Cr coating.

Table 1: Chemical composition of CrNi3MoVA steel[17]

C	Mn	Si	Cr	Ni	Mo	V	S	P
0.40	0.41	0.25	1.28	3.14	0.37	0.20	0.001	0.012

Table 2: Process parameters of AIP Cr coating

Arc current (A)	Duty cycle (%)	Deposition time (min)	Bias voltage (V)	Temperature (°C)
80	20	80	–250	150–200

The friction and wear properties of the Cr coating were tested using an HSR-2M high-speed reciprocating friction tester. One of the elements of the wear pair was a 304 stainless steel ball with a diameter of 6 mm, and the other was the Cr coating with dimensions of (20 × 10 × 5) mm. The hardness of the 304 stainless steel ball is 210 HV and its roughness is 0.6 μm. Due to its low hardness, the 304 stainless steel can be used as the band material for high-velocity projectiles. During rubbing, the Cr coating was fixed while the 304 stainless steel ball was sliding reciprocally. The parameters of the friction and wear test were as follows: the load was (3, 6 and 9) N, the sliding speed was 0.0417 m/s, the reciprocating distance was 5 mm, the total rubbing time was 1200 s, the total rubbing distance was 50 m, the test temperature was 22–25 °C, and the air humidity was 35–48 %. The corresponding initial contact pressures were (342, 430 and 493) MPa when the load was (3, 6 and 9) N.[21] The friction coefficient was recorded automatically using a tribometer, and all the values were the average of three tests to guarantee the stability and repeatability of the test results. The morphology of the Cr coating before and after the friction test was observed with a scanning electron microscope (SEM), the chemical composition of the worn area was investigated via energy-dispersive X-ray analysis (EDX), and the phase of the Cr coating was characterized with X-ray diffusion (XRD). In order to exclude the effect of adhesive material from the 304 stainless steel counter-ball on the mechanism of the Cr coating, the worn surface of the Cr coating was cleaned in anhydrous ethanol and acetone mixture for 10 min.

Figure 1 shows the sliding friction finite element model of the 304 stainless steel ball and the Cr coating. As shown in the figure, the two-dimensional plane model, coupled with temperature and displacement fields of the 304 stainless steel ball and the Cr coating, was established using ABAQUS numerical simulation software while the Coulomb friction model was chosen to simulate the rubbing process. The material properties of the 304 stainless steel and the Cr coating are listed in Table 3. Based on the test results for the friction coefficient, the stress distribution of the Cr coating under different loads was simulated to discuss the load influence on the friction and wear behavior of the Cr coatings.

Table 3: Material properties of the 304 stainless steel and Cr coating

Materials	Density (kg/m^3)	Young's modulus MPa	Poisson's ratio	Yield stress MPa	Plastic strain MPa
304 stainless steel	$8E^3$	$1.93E^5$	0.27	310	1000
Cr coating	$7.2E^3$	$2.7E^4$	0.2	350	500

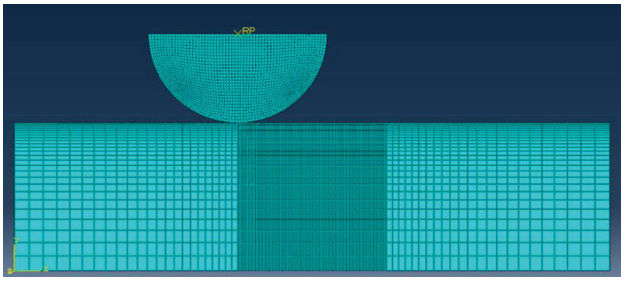

Figure 1: Sliding friction finite element model of the 304 stainless steel ball and Cr coating

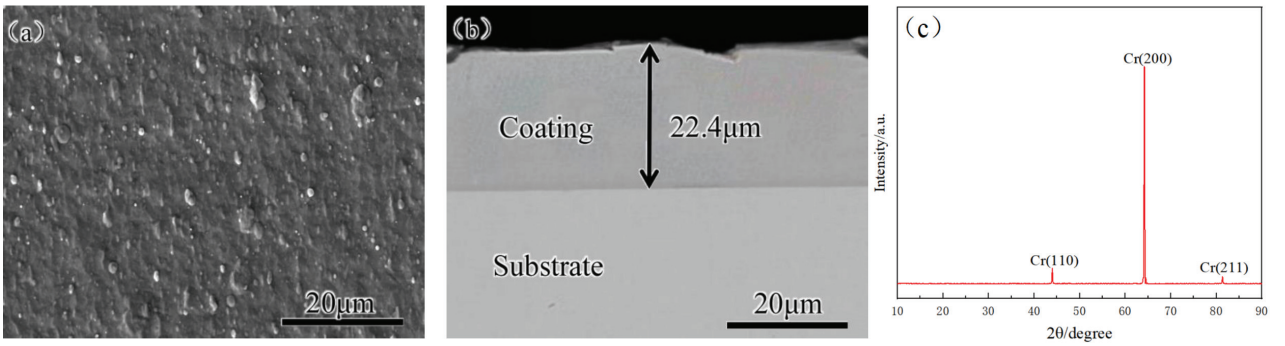

Figure 2: a) Surface, b) cross-section morphologies, c) XRD pattern of the Cr coating

3 RESULTS

3.1 Microstructure of Cr coating

Figure 2 shows the surface, cross-section morphologies, and XRD pattern of the Cr coating. As shown in **Figure 2a**, the surface of the Cr coating is a bit rough, which is very common for the coatings fabricated with AIP. The presence of microscopic droplets can be clearly observed on the Cr coating and the droplet size is mainly below 5 μm. It can be seen in **Figure 2b** that the Cr coating adheres closely to the substrate, and there are no cracks or delamination defects at the coating-substrate interface, while the thickness of the Cr coating is about 20 μm.

The XRD pattern (**Figure 2c**) shows that the three main diffraction peaks including Cr(110), Cr(200), and Cr(211) appear within the measurement angle range, of which the Cr(200) peak of the Cr coating exhibits the highest intensity, indicating a strong crystallographic orientation.

3.2 Tribological properties of Cr coating

Figure 3 shows the friction coefficients of the Cr coating under different loads. It can be observed that when the load is (3, 6 or 9) N, the average friction coefficient of the Cr coating is about 0.53, 0.47 and 0.34 respectively, indicating that with the increase in the load, the friction coefficient of the Cr coating is reduced. Furthermore, the friction coefficient of the Cr coating fluctuates slightly during steady rubbing when the load is 3 N and 6 N, while it decreased gradually from 0.41 to 0.29 when the load is 9 N.

Figure 4 shows 3D wear morphologies and 2D wear track profiles under the load of 3 N (a, b), 6 N (c, d) and 9 N (e, f). According to the 2D wear track profiles shown in **Figures 4b**, **4d** and **4f**, the depth and width of the wear tracks at different loads were obtained as listed in **Table 4**. According to this table, with the increase in the load, the depth and width of the wear track of the Cr coating firstly increases, and then decreases.

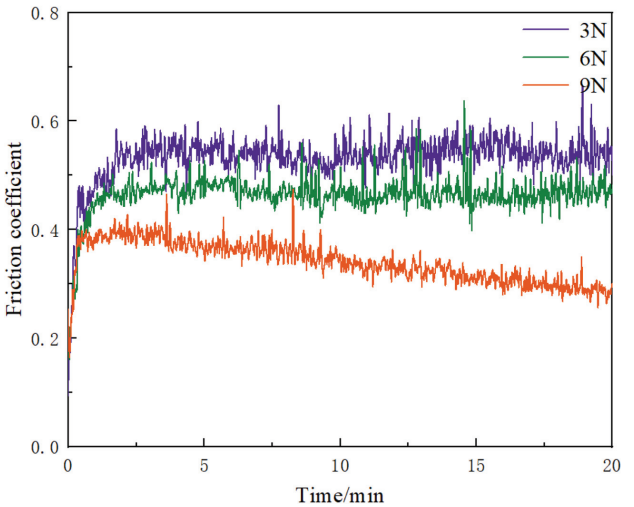

Figure 3: Friction coefficients of the Cr coating under different loads

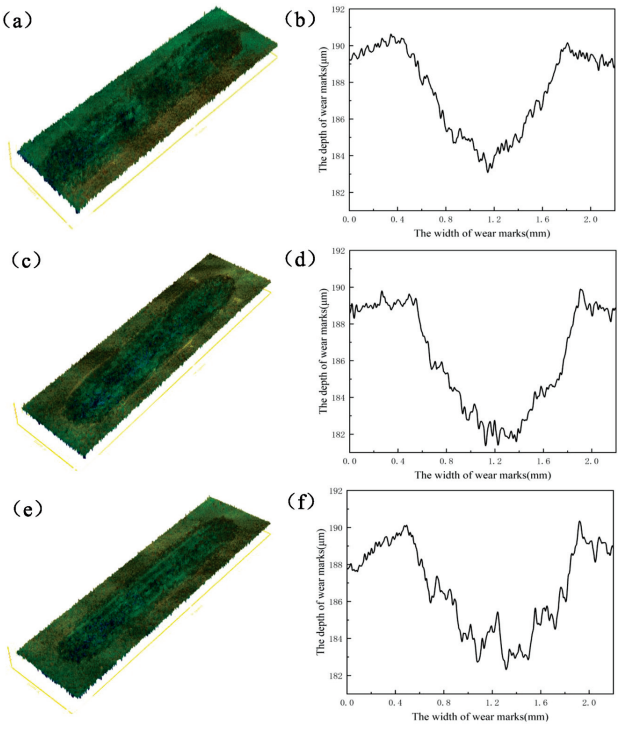

Figure 4: 3D wear morphologies and 2D wear track profiles under the loads of 3 N (a, b), 6 N (c, d) and 9 N (e, f)

Table 4: Depth and width of wear tracks at different loads

Load	Depth (μm)	Width (mm)
3 N	6.53	1.41
6 N	7.6	1.52
9 N	7.23	1.50

Wear rate (W, $mm^3N^{-1}m^{-1}$) can be evaluated based on the volume of wear track using the following equation:[22]

$$w = \frac{d^2 \times h\left\{2\times\arcsin\left(\frac{L}{D}\right) - \sin\left[2\times\arcsin\left(\frac{L}{D}\right)\right]\right\}}{8Fvt} \quad (1)$$

where d is the diameter of the rubbing ball, t is the rubbing time, v is the rubbing speed, F is the applied load, h is the length of the wear track, and L is the width of the wear track. According to Equation (1) and the width of the wear track (**Figure 4**), the wear rate of the Cr coating under different loads was calculated as shown in **Figure 5**. It can be seen in this figure that when the load is (3, 6 and 9) N, the average wear rate of the Cr coating is about (6.98×10^{-2}, 3.77×10^{-2} and 2.48×10^{-2}) $mm^3 \cdot N^{-1} \cdot m^{-1}$, respectively, indicating that with the increase in the load, the wear rate of the Cr coating is reduced.

3.3 Wear mechanism of Cr coating

The wear mechanism of the Cr coating during rubbing can be determined via SEM and EDX. **Figure 6** shows worn morphologies of the Cr coating at low and high magnification under different loads while **Table 5** shows EDX results for the worn surface at different positions under different loads from **Figure 6**. As shown in

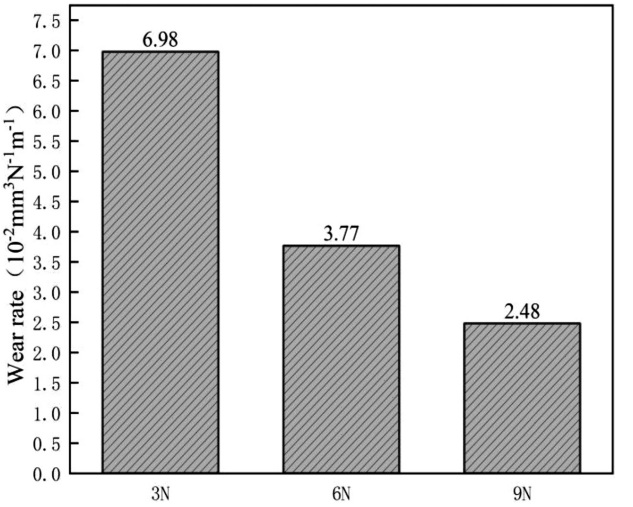

Figure 5: Wear rate of the Cr coating under different loads

Figure 6a, there are superficial layer spallation and plastic deformation sparsely distributed on the worn surface of the Cr coating, combining with the wear (**Figure 5**). This suggests that the wear mechanism of the Cr coating under the load of 3 N can be characterized as severe adhesive wear. EDX results for points A and B (**Figure 6b**) from the rectangle region from **Figure 6a**, examined at the high magnification, show that the wear debris contains 48.91 φ/% of the O element, 30.02 φ/% of the Cr element and 20.07 φ/% of the Fe element. On the other hand, the worn surface of the Cr coating contains 3.04 φ/% of the O element, 96.59 φ/% of the Cr element and 0.36 φ/% of the Fe element, indicating that the oxidation of the wear debris from the stainless ball takes place, while the surface of the Cr coating is hardly oxidized.

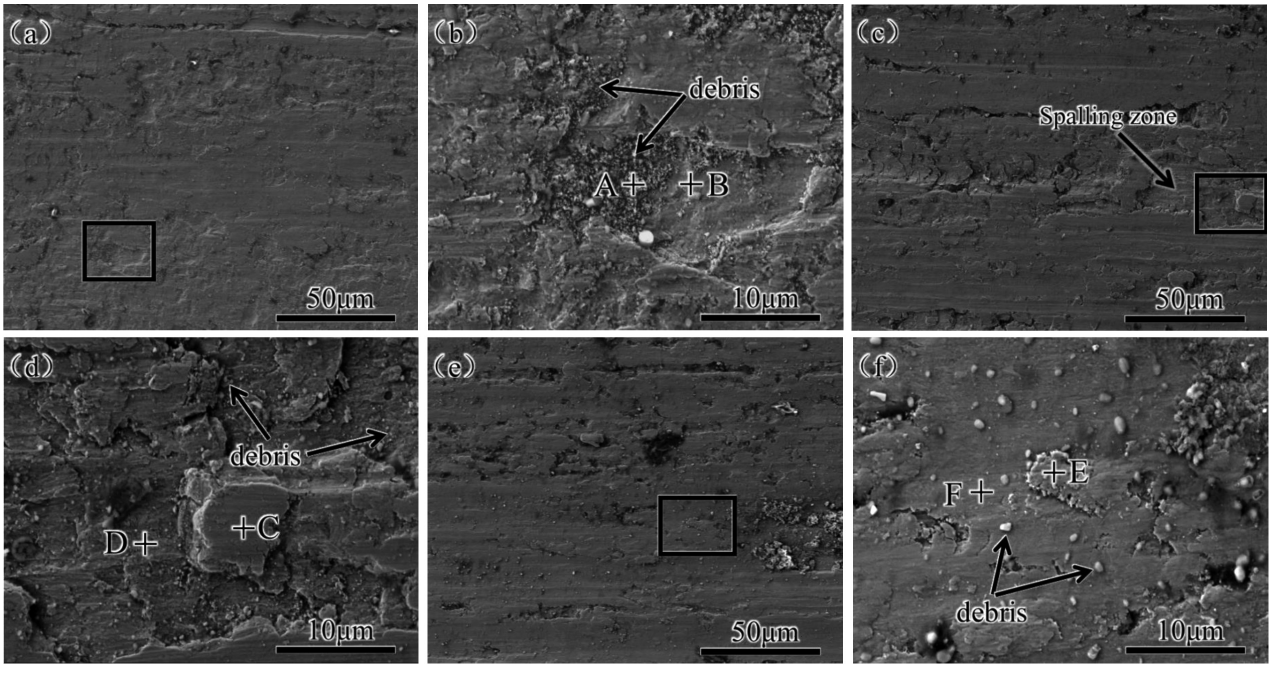

Figure 6: Worn morphologies of the Cr coating at low and high magnification under the loads of 3 N (a, b), 6 N (c, d) and 9 N (e, f)

Figure 6c shows the worn surface of the Cr coating under the load of 6 N. There are deep layer spallation and big plastic deformation on the worn surface of the Cr coating, suggesting that the wear of the Cr coating under the load of 6 N is also a type of severe adhesive wear. EDX results for points C and D (**Figure 6d**) from the rectangle region from **Figure 6c**, examined at the high magnification, show that the wear debris contains 17.51 φ/% of the O element, 53.72 φ/% of the Cr element and 28.73 φ/% of the Fe element, while the worn surface of the Cr coating contains 8.31 φ/% of the O element, 91.27 φ/% of the Cr element and 0.42 φ/% of the Fe element. The content of the O element in the wear debris under the load of 6 N is obviously lower than that under the load of 3 N, indicating that the wear debris of the former contains the spallation of the Cr coating. Moreover, the content of the O element on the surface of the Cr coating under the load of 6 N is higher than that under the load of 3 N, suggesting that the oxidation of the Cr coating accelerates with the increase in the load.

Figure 6e shows the worn surface of the Cr coating under the load of 9 N. There is less superficial layer spallation under the load of 9 N, and no deep layer spallation comparable to that from **Figure 6a** under the load of 3 N and **Figure 6c** under the load of 6 N. Therefore, the wear mechanism of the Cr coating under the load of 9 N is mild adhesive wear. EDX results for points E and F (**Figure 6f**) from the rectangle region from **Figure 6e** observed at the high magnification shows that the wear debris contains 40.40 φ/% of the O element, 25.36 φ/% of the Cr element and 34.23 φ/% of the Fe element. On the other hand, the worn surface of the Cr coating contains 23.87 φ/% of the O element, 64.53 φ/% of the Cr element and 11.60 φ/% of the Fe element, indicating that a thick tribofilm containing more oxides forms under the load of 9 N and is remarkably different from those formed at the loads of 3 N and 6 N during the rubbing.

Table 5: EDX results for the worn surface at different positions under different loads

Place	O content (φ/%)	Cr content (φ/%)	Fe content (φ/%)
A	48.91	30.02	20.07
B	3.04	96.59	0.36
C	17.51	53.72	28.73
D	8.31	91.27	0.42
E	40.40	25.36	34.23
F	23.87	64.53	11.60

3.4 Worn morphologies of 304 stainless steel counter-ball

Figure 7 shows the worn morphologies of the 304 stainless steel counter-ball at low and high magnification under the loads of 3 N (a, b, c), 6 N (d, e, f) and 9 N (g,

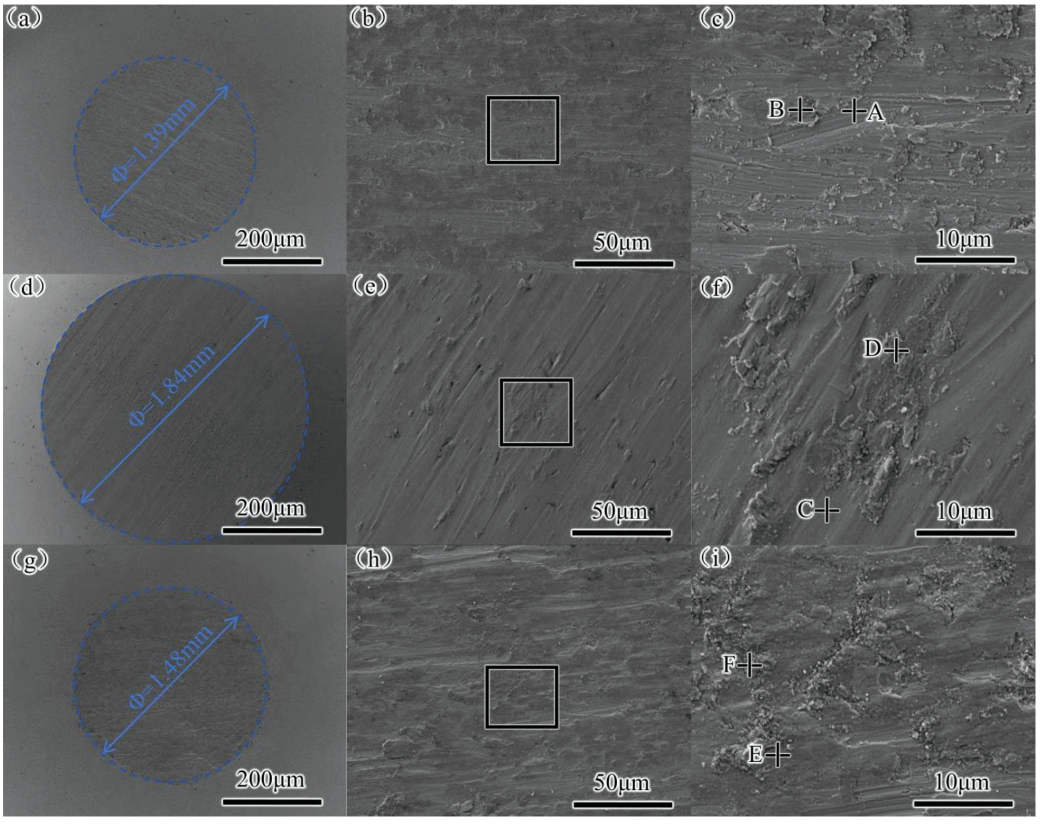

Figure 7: Worn morphologies of the 304 stainless steel counter-ball at low and high magnification under the loads of 3 N (a, b, c), 6 N (d, e, f) and 9 N (g, h, i)

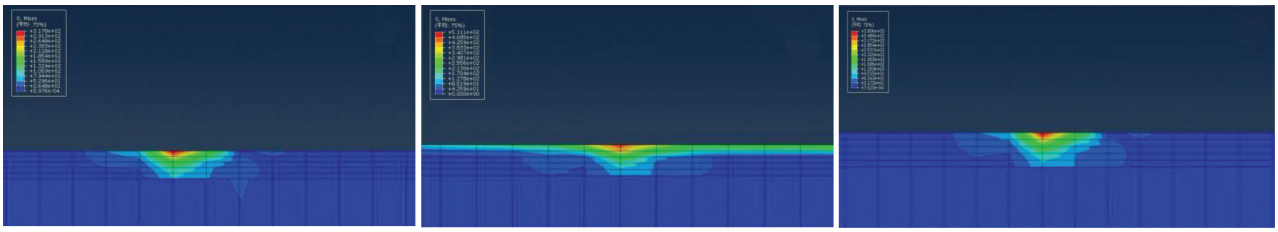

Figure 8: Cloud maps of stress field distribution in the rubbing zone of the Cr coating under different loads: a) 3 N, b) 6 N, c) 9 N

h, i). As shown in **Figures 7a**, **7d** and **7g**, with the increase in the load, the worn radius of the 304 stainless steel counter-ball first increases and then decreases, which is similar to the trend of the Cr coating. In order to clarify the mechanism of the Cr coating, the worn surface of the 304 stainless steel counter-ball was magnified and analyzed using EDX. As shown in **Figures 7c**, **7f** and **7i**, the adhesive feature appears on the surface of the 304 stainless steel counter-ball, and especially its worn surface under the 6 N load is much smoother than those under the 3 N and 9 N loads. In addition, there is more adhesive material on the worn surface under 9 N than on the worn surface under 3 N.

The chemical compositions of the worn surface of the 304 stainless steel counter-ball and wear debris were analyzed as shown in **Table 6**. With the increase in the load, the oxide in the wear debris of the 304 stainless steel counter-ball obviously increases. Furthermore, unlike the worn surface under 3 N and 6 N loads, the worn surface of the 304 stainless steel counter-ball under 9 N forms a tribofilm of oxides, which is similar to that on the worn surface of the Cr coating.

Table 6: EDX results for the worn surface at different positions and under different loads

Place	O content (φ/%)	Cr content (φ/%)	Fe content (φ/%)	Ni content (φ/%)
A	2.4	23.11	67.70	6.79
B	20.59	30.52	44.14	4.75
C	–	16.43	82.47	1.09
D	30.77	13.89	54.57	0.76
E	37.77	23.42	34.93	3.88
F	34.91	29.44	32.41	3.24

3.5 Simulation of stress field distribution across Cr coating in rubbing zone

Figure 8 shows cloud maps of the stress field distribution in the rubbing zone of the Cr coating under different loads. The increase in the load from 3 N to 6 N results in a sharp increase in the maximum equivalent stress of the rubbing zone on the surface of the Cr coating from 317.8 MPa to 511.1 MPa. Subsequently, the load further increases from 6 N to 9 N, leading to a decrease in the maximum equivalent stress of the rubbing zone on the surface of the Cr coating from 511.1 MPa to 380.6 MPa. The Coulomb friction model mainly reflects the influence of normal pressure and friction coefficient on the stress distribution. Simulated results indicate that the stress change is not only related to the loads, but also closely connected with the change in the friction coefficient. Due to the highest stress distribution, the greatest depth and width of the wear track took place at 6 N among the three loads.

4 DISCUSSION

S. K. Ghosh et al.[19] studied the tribological performance of an electroplated hard chromium coating on 17-4 PH steel with a ball-on-flat tribometer against an AISI 440C counterbody. The reciprocating motion occurred at three different frequencies (5, 10 and 15) Hz, and the slip amplitude was 1 mm with five different normal loads ranging from 3 N to 11 N. They found that the applied loads had a significant influence on the friction coefficient, particularly in relation to the worn material on the wear tracks. Therefore, friction and wear are not material properties, but rather responses of the system. Working conditions have a significant impact on the interface wear.

Z. X. Zeng el al.[20] investigated the tribological behavior of electroplated chromium coatings using a pin-on-plate SRV wear tester against a steel ball with a hardness of 700 HV. The experiments were carried out at a load of 60 N, a frequency of 25 Hz, and an amplitude of 1 mm. They proposed that Cr reacts with O_2 from air to form oxide particles during rubbing, and that these oxide particles have a notable impact on the wear mechanism of the Cr coating. K. Hiratsuka and K. Muramoto[23] proposed that small wear particles are generated during the severe wear stage, which are then easily oxidized in the subsequent rubbing stage. The attachment of oxidized wear particles to the worn surface forms an oxide film, which leads to mild wear. C. Guo et al.[24] investigated the friction and wear of an electropark-deposited AlCoCrFeNi high-entropy alloy coating using a reciprocating friction and wear testing machine with a GCr15 steel ball as the counter-body. A reciprocating distance of 10 mm, a reciprocating speed of 1000 rpm, a load of 10 N and ta otal friction time of 5 min showed that the excellent wear resistance of the AlCoCrFeNi coating is due to the oxide scales formed on the coating surface during rubbing, exhibiting excellent adherence and playing a role in self-lubrication. The above investigations indicate that oxidized wear particles that strongly adhere to the rubbing contact surface are necessary for the se-

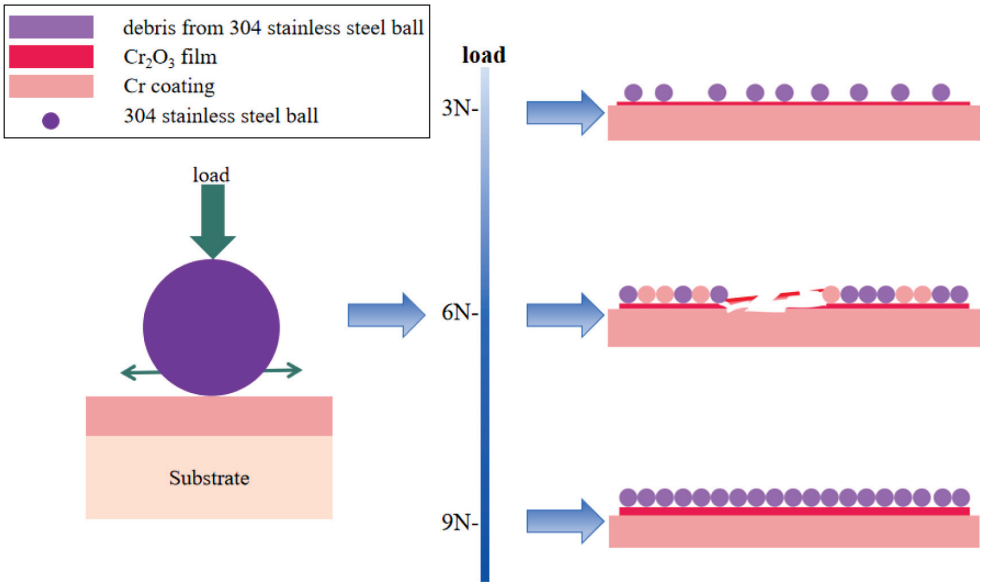

Figure 9: Schematic of the wear mechanism of the Cr coating under different loads

vere-to-mild wear transition, along with the oxide scales formed by the heat produced during rubbing. Furthermore, H. Kato[25] suggested that the severe-to-mild wear transition occurs when the relative area of the oxide film reaches a critical value, which is proportional to the real contact area.

As the 304 stainless steel ball has a lower strength than the Cr coating, during the running-in stage of the metal-to-metal contact, severe adhesion wear occurred according to the worn morphologies of the 304 stainless steel counter-ball (**Figure 8**). Metallic wear debris was generated at the rubbing interface and broken into small wear particles, which were prone to oxidation due to the high temperature resulting from frictional heat under the high load of 9 N (**Table 7**). The main chemical reactions involving the wear debris from the 304 stainless steel ball are as follows:

$$4Fe + 3O_2 = 2Fe_2O_3 \quad (2)$$

$$4Cr + 3O_2 = 2Cr_2O_3 \quad (3)$$

Meanwhile, the surface of the Cr coating was also oxidized due to frictional heat as Cr has a strong affinity for O. With the increase in the load, the oxidation of the Cr coating accelerates (**Table 6**), which is beneficial for the hardening of the surface material of the Cr coating. Therefore, the wear mechanism of the Cr coating under different loads can be proposed as schematically illustrated in **Figure 9**. As shown in this figure, under the load of 3 N, there are sparsely distributed oxides from the wear debris of the 304 stainless steel ball on the worn surface the of Cr coating, which remained largely unoxidized during rubbing. The tribofilm area does not reach the critical value and has no anti-friction effect. Under the load of 6 N, as the stress in the rubbing zone sharply increases (**Figure 8**), deep layer spallation of the Cr coating surface occurs, causing the real contact area to increase. This leads to a wear increase. Under the load of 9 N, with the increase in the load, the temperature caused by frictional heat increases, which accelerates the oxidation of both the wear debris and the surface of the Cr coating, as well as the hardening of the surface material of the Cr coating. Finally, mild wear is established in the tribofilm area as it reaches the critical value.

5 CONCLUSIONS

When the initial contact pressure is (342, 430 and 493) MPa, the friction coefficient of the Cr coating is about 0.53, 0.47 and 0.34 whilst its wear rate is about (5.78×10^{-2}, 3.37×10^{-2} and 2.11×10^{-2}) $mm^3 \cdot N^{-1} \cdot m^{-1}$, respectively.

When the initial contact pressure is (342, 430 and 493) MPa, the maximum equivalent stress of the rubbing zone on the surface of the Cr coating is (317.8, 511.1 and 380.6) MPa according to the simulated results based on the Coulomb friction model.

When the initial contact pressure increases from 342 MPa to 430 MPa, a severe-to-mild adhesive wear mechanism transition occurs in the Cr coating. It takes place in the tribofilm area as the contact interface reaches a critical pressure of 493 MPa, accompanied by oxidation and hardening of the surface material of the Cr coating.

Acknowledgment

The authors are grateful for the financial support from the Research Project of Application Foundation of Liaoning Province of China (No.2022JH2/101300006), the Research Project of Education Department of Liaoning Province of China (LJKMZ20220604 and 1030040000675), the Special Fund of Basic Scientific Research Operating Expense of Undergraduate Univer-

sities in Liaoning Province, and Key Laboratory of Weapon Science & Technology Research (LJ232410144071), the Light-Selection Team Plan of Shenyang Ligong University and the Foundation of National Key Laboratory for Remanufacturing.

6 REFERENCES

[1] Y. Meng, C. Chen, S. Zeng, C. Zhu, X. Zhou, X. Han, Investigations of oxidation behavior and establishment of life-cycle model during the steam oxidation of Cr-coated Zry-4 at 1200°C, Corrosion Science, 226 (**2024**), 111694, doi:10.1016/j.corsci.2023.111694

[2] Q. Li, P. Song, R. Zhang, Z. Li, Y. Wang, P. Du, J. Lu, Oxidation behavior and Cr-Zr diffusion of Cr coatings prepared by atmospheric plasma spraying on zircaloy-4 cladding in steam at 1300°C, Corrosion Science, 203 (**2022**), 110378, doi:10.1016/j.corsci.2022.110378

[3] P. Shukla, S. Awasthi, J. Ramkumar, K. Balani, Protective trivalent Cr-based electrochemical coatings for gun barrels, Journal of Alloys and Compounds, 768 (**2018**), 1039–1048, doi:10.1016/j.jallcom.2018.07.170

[4] R. Bayón, A. Igartua, X. Fernández, R. Martínez, R. J. Rodríguez, J. A. García, A. de Frutos, M. A. Arenas, J. de Damborenea, Corrosion-wear behaviour of PVD Cr/CrN multilayer coatings for gear applications, Tribology International, 42 (**2009**) 4, 591–599, doi:10.1016/j.triboint.2008.06.015

[5] C. Larson, J. R. Smith, Recent trends in metal alloy electrolytic and electroless plating research: a review, Transactions of the IMF, 89 (**2011**) 6, 333–341, doi:10.1179/174591911X13171174481239

[6] A. Brenner, Electrodeposition of Alloys, 1nd ed., Elsevier, New York 1963

[7] S. Wang, C. Ma, F. C. Walsh, Alternative tribological coatings to electrodeposited hard chromium: a critical review, Transactions of the IMF, 98 (**2020**) 4, 173–185, doi:10.1080/00202967.2020.1776962

[8] Y. Deng, W. L. Chen, B. X. Li, C. Y. Wang, T. C. Kuang, Y. Q. Li, Physical vapor deposition technology for coated cutting tools: A review, Ceramics International, 46 (**2020**) 11, 18373–18390, doi:10.1016/j.ceramint.2020.04.168

[9] C. W. Chien, C. L. Liu, F. J. Chen, K. H. Lin, C. S. Lin, Microstructure and properties of carbon–sulfur-containing chromium deposits electroplated in trivalent chromium baths with thiosalicylic acid, Electrochimica Acta, 72 (**2012**), 74–80, doi:10.1016/j.electacta.2012.03.168

[10] S. Xie, Water contamination due to hexavalent chromium and its health impacts: exploring green technology for Cr (VI) remediation, Green Chemistry Letters and Reviews, 17 (**2024**) 1, doi:10.1080/17518253.2024.2356614

[11] J. Liu, X. Zhang, V. Pelenovich, Y. Xu, K. Tan, L. W. Hu, X. M. Zeng, Z. Zeng, Y. Lei, Y. M. Chen, B. Yang, Effects of duty cycle on microstructure and mechanical properties of (AlCrNbSiTi) N high-entropy nitride hard coatings deposited by pulsed arc ion plating, Vacuum, 225 (**2024**), 113219, doi:10.1016/j.vacuum.2024.113219

[12] J. J. Wu, M. L. Shen, M. Hu, C. Guo, Q. Li, S. L. Zhu, High vacuum arc ion plating Cr films: Self-ion bombarding effect and oxidation behavior, Corrosion Science, 187 (**2021**), 109476, doi:10.1016/j.corsci.2021.109476

[13] M. Hu, M. L. Shen, Z. L. Liu, C. Guo, Q. Li, S. L. Zhu, Self-ion bombarded Cr films: Crystallographic orientation and oxidation behaviour, Corrosion Science, 143 (**2018**), 212–220, doi:10.1016/j.corsci.2018.08.016

[14] M. Hu, M. F. Pan, M. L. Shen, C. Guo, Y. Y. Tang, H. J. Yu, Thermal shock behaviour and failure mechanism of two-kind Cr coatings on non-planar structure, Engineering Failure Analysis, 141 (**2022**), 106697, doi:10.1016/j.engfailanal.2022.106697

[15] H. L. Yang, X. M. Chen, L. Chen, Z. J. Wang, G. C. Hou, C. A. Guo, J. Zhang, Influence of temperature on tribological behavior of AlCoCrFeNi coatings prepared by electrospark deposition, Digest Journal of Nanomaterials & Biostructures (DJNB), 18 (**2023**) 1, doi:10.15251/DJNB.2023.181.145

[16] T. X. Liu, C. A. Guo, F. S. Lu, X. Y. Zhang, L. Zhang, Z. J. Wang, Z. Y. Xu, G. L. Zhu, Influence of deposition voltage on tribological properties of W-WS2 coatings deposited by electrospark deposition, Chalcogenide Letters, 20 (**2023**) 10, doi:10.15251/CL.2023.2010.741

[17] Z. Wang, G. Zhu, F. Lu, L. Zhang, Y. Wang, S. Zhao, C. Guo, J. Zhang, Friction and Wear Performance of an Electrospark-Deposited Ta Coating on CrNi3MoVA ST, Materials and Technology, 58 (**2024**) 1, 17–23, doi:10.17222/mit.2023.894

[18] W. Y. Fei, S. X. Sheng, G. Jie, S. Y. Hua, G. L. Yuan, Z. Y. Qing, Surface crack propagation of electroplated chromium coating and cotton fabric with dry friction, Engineering Failure Analysis, 163 (**2024**), 108485, doi:10.1016/j.engfailanal.2024.108485

[19] S. K. Ghosh, P. K. Limaye, C. Srivastava, A. K. Sahu, Investigation of tribological and corrosion performance of electroplated hard chromium coating on 17-4 PH steel, Surface Engineering, 39 (**2023**) 5, 521–531, doi:10.1080/02670844.2023.2247862

[20] Z. Z. Xiang, W. L. Ping, C. Li, Z. J. Yan, The correlation between the hardness and tribological behaviour of electroplated chromium coatings sliding against ceramic and steel counterparts, Surface and Coatings Technology, 201 (**2006**) 6, 2282–2288, doi:10.1016/j.surfcoat.2006.03.038

[21] A. C. Fischer-Cripps, Introduction to Contact Mechanics, 2nd ed., Springer, New York 2007

[22] Q. Wang, M. Chen, Z. Shan, C. Sui, L. Zhang, S. Zhu, F. Wang, Comparative study of mechanical and wear behavior of Cu/WS2 composites fabricated by spark plasma sintering and hot pressing, Journal of Materials Science & Technology, 33 (**2017**) 11, 192–199, doi:10.1016/j.jmst.2017.06.014

[23] K. Hiratsuka, K. Muramoto, Role of wear particles in severe–mild wear transition, Wear, 259 (**2005**) 1–6, 467–76, doi:10.1016/j.wear.2005.02.102

[24] C. Guo, Z. Zhao, F. Lu, B. Zhao, S. Zhao, J. Zhang, Performance of high-speed friction and wear of electrospark deposited AlCoCrFeNi high-entropy alloy coating, Digest Journal of Nanomaterials and Biostructures, 13 (**2018**) 4, 931–939

[25] H. Kato, Effects of supply of fine oxide particles onto rubbing steel surfaces on severe–mild wear transition and oxide film formation, Tribology International, 41 (**2008**) 8, 735–742, doi:10.1016/j.triboint.2008.01.001